Collective Chemotactic Dynamics in the Presence of Self-Generated Fluid Flows

Enkeleida Lushi[1,2], Raymond E. Goldstein[3], Michael J. Shelley[1]

[1]*Courant Institute of Mathematical Sciences, New York University, NY, USA*
[2]*Department of Mathematics, Imperial College London, London, UK*
[3]*Department of Applied Mathematics and Theoretical Physics, University of Cambridge, Cambridge, UK*

In micro-swimmer suspensions locomotion necessarily generates fluid motion, and it is known that such flows can lead to collective behavior from unbiased swimming. We examine the complementary problem of how chemotaxis is affected by self-generated flows. A kinetic theory coupling run-and-tumble chemotaxis to the flows of collective swimming shows separate branches of chemotactic and hydrodynamic instabilities for isotropic suspensions, the first driving aggregation, the second producing increased orientational order in suspensions of "pushers" and maximal disorder in suspensions of "pullers". Nonlinear simulations show that hydrodynamic interactions can limit and modify chemotactically-driven aggregation dynamics. In puller suspensions the dynamics form aggregates that are mutually-repelling due to the non-trivial flows. In pusher suspensions chemotactic aggregation can lead to destabilizing flows that fragment the regions of aggregation.

A growing body of experimental work has established that suspensions of motile microorganisms can develop complex large-scale patterns of collective swimming at sufficiently high concentration [1, 2]. This behavior generally occurs in the *absence* of directional cues for swimming, purely as a consequence of steric and hydrodynamic interactions between the cells. Yet, there are many circumstances in which cells exhibit chemotaxis, directed motion in response to chemical gradients, and this process by itself can lead to complex spatio-temporal pattern formation [3]. As swimmer-generated flows may also advect any chemoattractant field, it is natural then to ask how self-generated fluid flows in suspensions of microorganisms affect modes of communication [4] and aggregation. Here we present an analysis of this issue and suggest potential realizations of this pattern-forming system.

Chemotactic focusing of cell concentration has been studied using the classical Keller-Segel (KS) model [5] and in theories incorporating the run-and-tumble (RT) [6] dynamics of bacterial motion [7, 8]. We extend a well-known kinetic model for modulated RT dynamics to include flows produced by the active stresses due to swimming. A simpler version of our model is considered in [7] to study swimmer transport and rotation in a given background shear flow. Without RT dynamics, our model reduces to one for active suspensions [9] which captures the large-scale flows seen in experiments [1, 10] and illuminates the effect of propulsion mechanism (*pusher* vs. *puller*) on large-scale dynamics and stability. When swimmers produce a chemoattractant leading to aggregation, the self-generated flows can have a large effect; pushers create complex flows that can bound growth in organism density, while pullers show limited pattern coarsening and isolated aggreggates repelling due to non-trivial flows. Merging the RT and active suspension models is seamless as both are kinetic theories with conformation variables the particle position and orientation [11].

Consider a suspension of swimmers at local concentration $\Phi(\mathbf{x}, t)$, each of which moves at a constant speed U in a run-and-tumble dynamics. They move in a fluid of local velocity $\mathbf{u}(\mathbf{x}, t)$ and produce a chemoattractant of concentration $C(\mathbf{x}, t)$ and molecular diffusivity D_C. We choose rescalings based on the swimmer contribution to the fluid stress tensor (below), with a characteristic length $\ell = l/\phi$, where l is the swimmer size and $\phi \equiv l^3 \langle \Phi \rangle$ is the effective mean volume fraction in suspension. Scaling time by ℓ/U, C evolves as

$$C_t + \mathbf{u} \cdot \boldsymbol{\nabla} C = Pe^{-1} \nabla^2 C - \beta_1 C + \beta_2 \Phi \ , \qquad (1)$$

where β_1 and β_2 are rate constants for chemoattractant self-degradation and production, and the Péclet number $Pe = U\ell/D_C$ measures the strength of diffusion to advection on the intrinsic scale ℓ. Collective swimming may generate coherence on larger scales with higher speeds, increasing the importance of advection. Without advection this is the KS model [5]. In the case of *E. coli* [12] gives $U \sim 25~\mu\text{m/s}$, $l \sim 5~\mu\text{m}$, $\phi \sim 0.1$ at a cell concentration of $10^9~\text{cm}^{-3}$, so $\ell \sim 50~\mu\text{m}$. With $D_C \sim 5 \times 10^{-6}~\text{cm}^2/\text{s}$ we obtain $Pe \simeq 2.5$, $\beta_1 \simeq 0.008$ and $\beta_2 \simeq 0.004$. For faster-swimming organisms, such as marine bacteria [13], this intrinsic Péclet number can reach $\mathcal{O}(10-20)$.

The configuration of swimmers is given by a distribution function $\Psi(\mathbf{x}, \mathbf{p}, t)$ of the center of mass position $\mathbf{x}$ and orientation $\mathbf{p}$ satisfying the Fokker-Planck equation

$$\Psi_t = - \left[\lambda(\mathcal{D}_t C)\Psi - \frac{1}{4\pi} \int d\mathbf{p}' \lambda(\mathcal{D}_t C)\Psi(\mathbf{x}, \mathbf{p}', t) \right]$$
$$- \boldsymbol{\nabla}_{\mathbf{x}} \cdot (\Psi \dot{\mathbf{x}}) - \boldsymbol{\nabla}_{\mathbf{p}} \cdot (\Psi \dot{\mathbf{p}}) \ , \qquad (2)$$

where the local swimmer concentration is $\Phi(\mathbf{x}, t) = \int d\mathbf{p}\Psi(\mathbf{x}, \mathbf{p}, t)$. The bracketed term in (2) describes the effect of RT chemotaxis based on a swimming dynamics of straight runs and modulated reorientations (tumbles) where $\lambda(\mathcal{D}_t C)$ is a tumbling frequency, the probability of
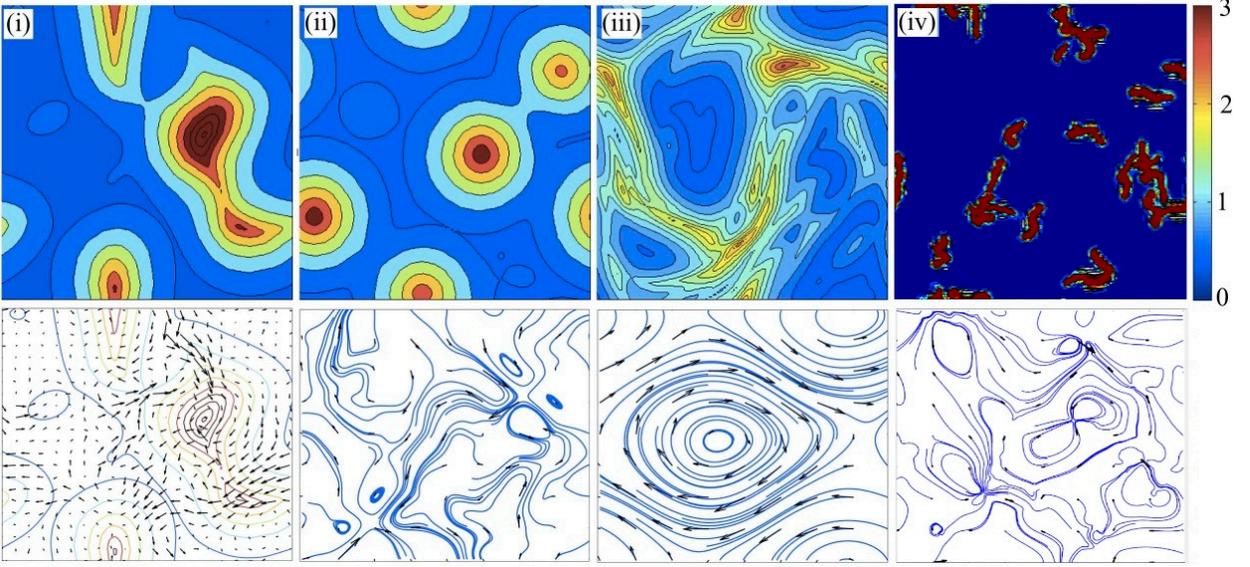
FIG. 1: (color online). Chemotactic suspensions at large times, $t = 3000$. Swimmer concentration Φ (top) and mean direction $\mathbf{n}$ (bottom) for (i) chemotactic neutral swimmers ($\mathbf{u} = 0$), and (ii) Φ (top), fluid streamlines and velocity field $\mathbf{u}$ (bottom) for chemotactic pullers. (iii,iv) Φ (top), streamlines and $\mathbf{u}$ (bottom) for chemotactic pushers. Parameters $\beta_1 = \beta_2 = 0.25$, $Pe = 20$, $\gamma = 1$, $D_T = D_R = 0.025$. Parameters λ_0 and χ are indicated in Figs. 2c,d for cases (i-iii) and are $\lambda_0 = 5, \chi = 0.6$ for case (iv). See [16] for movies of swimmer concentration dynamics.

a bacterial tumble event as a function of the chemoattractant temporal gradient $\mathcal{D}_t C = C_t + (\mathbf{p} + \mathbf{u}) \cdot \boldsymbol{\nabla} C$ along a swimmer's path. Experiments [14] show that when $\mathcal{D}_t C > 0$ the tumbling frequency is reduced, and is otherwise constant, as captured by the biphasic form $\lambda(\mathcal{D}_t C) = \lambda_0 \max(\min(1 - \chi \mathcal{D}_t C, 1), 0)$, a linearized version of an earlier model [8, 12]. The fluxes in (2) are

$$\dot{\mathbf{x}} = \mathbf{p} + \mathbf{u}, \qquad \dot{\mathbf{p}} = (\mathbf{I} - \mathbf{pp})\left(\gamma \mathbf{E} + \mathbf{W}\right)\mathbf{p}. \qquad (3)$$

The particle velocity $\dot{\mathbf{x}}$ includes swimming at constant speed (non-dimensionalized to unity) in the axis direction $\mathbf{p}$ ($|\mathbf{p}| = 1$), translation by the fluid velocity $\mathbf{u}$. (In the KS model [5], swimmer speed is linear in the chemical gradient.) The angular velocity $\dot{\mathbf{p}}$ follows Jeffrey's equation [15] where $\mathbf{E} = (\boldsymbol{\nabla}_{\mathbf{x}} \mathbf{u} + \boldsymbol{\nabla}_{\mathbf{x}} \mathbf{u}^T)/2$ is the rate-of-strain tensor, $\mathbf{W} = (\boldsymbol{\nabla}_{\mathbf{x}} \mathbf{u} - \boldsymbol{\nabla}_{\mathbf{x}} \mathbf{u}^T)/2$ is the vorticity tensor. For rod-like swimmers, the shape factor is $\gamma \sim 1$.

The fluid velocity $\mathbf{u}(\mathbf{x}, t)$ produced by the suspension satisfies the Stokes equations driven by an "active" stress $\boldsymbol{\Sigma}^a$ arising from particle locomotion:

$$- \nabla_{\mathbf{x}}^2 \mathbf{u} + \boldsymbol{\nabla}_{\mathbf{x}} q = \boldsymbol{\nabla}_{\mathbf{x}} \cdot \boldsymbol{\Sigma}^a, \qquad \boldsymbol{\nabla}_{\mathbf{x}} \cdot \mathbf{u} = 0 \qquad (4)$$

$$\boldsymbol{\Sigma}^a(\mathbf{x}, t) = \alpha \int d\mathbf{p}\,\Psi(\mathbf{x}, \mathbf{p}, t)\mathbf{pp}. \qquad (5)$$

The active stress is an orientational average of the force dipoles $\alpha \mathbf{pp}$ the cells exert on the fluid [9], where α is an $\mathcal{O}(1)$ constant by our rescaling. A cell that self-propels by front-actuation (a puller) has stresslet strength $\alpha > 0$, and a rear-actuated cell (pusher) has $\alpha < 0$. The case of "neutral" cells ($\alpha = \mathbf{u} = 0$) is the closest this model approaches the KS [5] and RT models [8, 12].

We first illustrate the effect hydrodynamics has on aggregation. From nonlinear simulations of Eqs. (1-6), Fig. 1 shows the swimmer concentration $\Phi(\mathbf{x}, t)$ and mean orientation $\mathbf{n} = \int d\mathbf{p}\Psi/\Phi$ at late times, having started near uniform isotropy, for neutral, puller, and pusher suspensions. All share a dominant self-aggregation instability, but differing (or no) hydrodynamic interactions. Neutral swimmers show aggregation and pattern coarsening. Pullers show limited aggregation into circular spots kept apart by non-trivial fluid flows. Pushers create complex fluid flows and fragmented aggregation regions.

These behaviors can be understood through a stability analysis of uniform isotropic suspensions. For simplicity, consider rod-like ($\gamma = 1$) swimmers and a quasi-static chemoattractant field $Pe^{-1}\nabla^2 C - \beta_1 C = -\beta_2 \Phi$, which slaves C to Φ. The tumbling frequency is simplified to $\lambda(\mathbf{p}) = \lambda_0 (1 - \chi \mathbf{p} \cdot \nabla C)$. A steady state is $\Psi_0 = 1/4\pi$ ($\Phi = 1$), $\mathbf{u} = \mathbf{0}$, and $C_0 = \beta_1/\beta_2$. Perturbations of the form $\epsilon(\tilde{\Psi}(\mathbf{p}, \mathbf{k}), \tilde{C}(\mathbf{k})) \exp(i\mathbf{k} \cdot \mathbf{x} + \sigma t)$, yield

$$(\sigma + \lambda_0 + i\mathbf{k} \cdot \mathbf{p})\tilde{\Psi} = \frac{\lambda_0}{4\pi}\left(\frac{ik\chi\beta_2(\hat{\mathbf{k}} \cdot \mathbf{p})}{\beta_1 + k^2 Pe^{-1}} + 1\right)\tilde{\Phi}$$
$$- \frac{3\alpha}{4\pi}(\hat{\mathbf{k}} \cdot \mathbf{p})\mathbf{p} \cdot (\mathbf{I} - \hat{\mathbf{k}}\hat{\mathbf{k}})\tilde{\boldsymbol{\Sigma}}^p \mathbf{k}, \qquad (6)$$

where $\tilde{\Phi} = \int d\mathbf{p}'\tilde{\Psi}'$ and $\mathbf{k} = k\hat{\mathbf{k}}$. Since $\tilde{\boldsymbol{\Sigma}}^p = \int d\mathbf{p}'\tilde{\Psi}'\mathbf{p}'\mathbf{p}'$, this is a linear eigenvalue problem for $\tilde{\Psi}$ and σ. The first term on the RHS is chemotactic (C) and has unstable dynamics restricted to the zeroeth azimuthal mode on $|\mathbf{p}| = 1$. The second is hydrodynamic (H), with unstable dynamics restricted to the first azimuthal mode. This
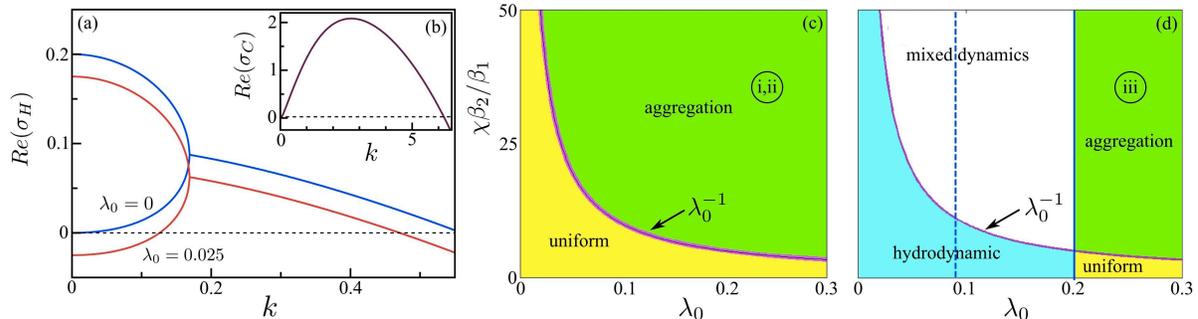
FIG. 2: (color online). Linear stability analysis. (a) Branches of the hydrodynamic instability, with and without tumbling, for pushers. (b) Chemotactic branch for $\chi = 35$, $\lambda_0 = 0.25$, $\beta_1 = \beta_2 = 1/4$ and $Pe = 20$. Regimes diagram for (c) neutral swimmers and pullers, and (d) pushers. Solid curves give linear stability boundaries for long waves. Dashed lines show shifted boundaries in nonlinear simulations at finite box size. Encircled labels (i-iii) denote parameters used in simulations (Fig. 1a-c).

yields *uncoupled* relations for growth rates $\sigma_{C,H}$,

$$\frac{2}{\lambda_0} = R\left[2 + a_C \log\left(\frac{a_C - 1}{a_C + 1}\right)\right] - \frac{1}{ik}\log\left(\frac{a_C - 1}{a_C + 1}\right)$$

$$\frac{4k}{3i\alpha} = 2a_H^3 - \frac{4}{3}a_H + (a_H^4 - a_H^2)\log\left(\frac{a_H - 1}{a_H + 1}\right) , \quad (7)$$

where $a_{C,H} = (\sigma_{C,H} + \lambda_0)/ik$ and $R = \chi\beta_2/(\beta_1 + k^2/Pe)$. We refer to these as the *chemotactic* and *hydrodynamic* relations, respectively. The first induces growth in concentration fluctuations, while the second increases orientational order. The two are coupled only through the basal tumbling rate λ_0 which in the hydrodynamic relation only shifts the growth rate. Further, the chemotactic instability gives rise to normal stresses of the form $\tilde{\mathbf{\Sigma}}^p = \hat{\mathbf{k}}\hat{\mathbf{k}} - \hat{\mathbf{k}}_\perp\hat{\mathbf{k}}_\perp$, while the hydrodynamic instability gives shear stresses of the form $\tilde{\mathbf{\Sigma}}^p = \hat{\mathbf{k}}\hat{\mathbf{k}}_\perp + \hat{\mathbf{k}}_\perp\hat{\mathbf{k}}$.

For pushers ($\alpha < 0$) the hydrodynamic instability has a finite bandwidth (Fig. 2a), though with maximal growth rates at $k = 0$. Tumbling shifts down the $Re(\sigma_H(k))$ branch by λ_0 for all k, further stabilizing the system. Long-wave asymptotics of (7) give two solution branches: $\sigma_{H1} \simeq -\alpha/5 - \lambda_0 + 15/7\alpha k^2$ and $\sigma_{H2} \simeq -\lambda_0 + O(-\alpha k^2)$. There is no hydrodynamic instability for pullers [9]. Fig. 2b shows the chemotactic growth rate. Small k asymptotics yields $\sigma_C \approx k^2/(3\lambda_0)[(\chi\beta_2/\beta_1)\lambda_0 - 1]$: for $(\chi\beta_2/\beta_1) > 1/\lambda_0$ there are wavenumbers with $Re(\sigma_C(k)) > 0$, shown in one case as a finite band of unstable modes whose width is controlled by chemo-attractant diffusion.

From Fig. 2a, we can obtain a range for λ_0 for which there is a hydrodynamic instability in pusher suspensions. Heuristically, λ_0 sets an effective rotational diffusivity, and $\lambda_0 \geq 0.2$ turns off the hydrodynamic instability for any system size. For $L = 50$ and the diffusion constants used in simulations, $\lambda_0 \geq 0.09$ suffices. This information is assembled in Fig. 2 c,d as phase diagrams that relate the parameters to various dynamical regimes.

Numerical studies of the full nonlinear dynamics (1–5) were done in 2D, with a box size $L = 50$ large enough to include several unstable linear modes. Swimmer translational and rotational diffusions are added in the model to control the growth of steep gradients over long-times. An initial random perturbation of the uniform isotropic state is used: $\Psi(\mathbf{x}, \mathbf{p}, 0) = 1/2\pi + \Sigma_i\epsilon_i\cos(\mathbf{k}_i\cdot\mathbf{x} + \xi_i)Q_i(\mathbf{p}_i)$ with random coefficients $|\epsilon_i| < 0.01$, ξ_i an arbitrary phase and Q_i a low-order polynomial. The initial chemo-attractant concentration is uniform with $C(\mathbf{x}, 0) = \beta_1/\beta_2 = 1$. Figure 1 shows long-time swimmer concentration Φ for four illustrative cases. In each case, concentration C closely tracks Φ. Cases (i-iii) share the same chemotactic instability, but differ in swimming actuation: $\alpha = 0, 1, -1$.

The expected regimes of these three cases are shown in Figs. 2c,d. For neutral swimmers, aggregation dominates and the dynamics is typified by the formation of a few regions of steadily increasing concentration that slowly coarsen (Fig. 1a). The maximum swimmer concentration (Fig. 3) shows little sign of the rapid self-focussing associated with finite-time chemotactic collapse [17] of the KS model, which here may be due to the fixed swimming speed [18]. While the initial aggregation for pullers (Fig. 1b) is similar to that for neutral swimmers (Fig. 3) its long-time behavior is very different. Concentration growth and coarsening cease as the dynamics enters a near steady-state with circular regions of high concentration. Active-stress driven flows suppress further coarsening by pushing nearby peaks apart and apparently maintain the few remaining high concentration regions.

For pushers (Fig. 1c), linear theory gives only a chemotactic instability, and the dynamics is indeed initially dominated by aggregation as is evidenced by the early rapid growth of normal stresses relative to shear stresses (not shown). However, aggregation into a regions with high swimmer concentration creates a destabilizing active stress, giving rise to unsteady fluid flows. These flows fragment the peaks while pushing them around the

4
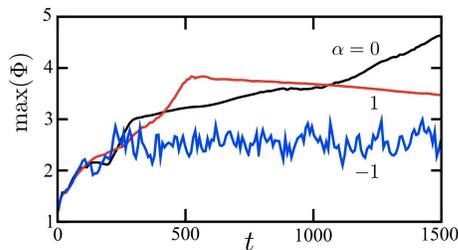
FIG. 3: (color online) Measures of growth: maximum swimmer concentration for cases (i-iii) in Fig. 1.

domain. The dynamics is one of constant aggregation and flow instability, which apparently suppresses further growth in swimmer concentration (Fig. 3).

Lastly, we examine in Fig. 1(iv) the dynamics that arises with parameters close to those measured by Saragosti *et al* [12] (before our rescaling) in their experiments of *E. coli* chemotaxis. These parameters lie far to the right of the aggregation regime of Fig. 2d as λ_0 is 20 times higher than at the predicted threshold for suppressing hydrodynamic instabilities. Not surprisingly, the simulations show chemotactic aggregation into very high peaks. Once the swimmer concentration in those peaks is large enough, the active stresses give rise to small-scale and localized fluid flows (cf. Fig. 1(iii)). These local flows do appear to be implicated in the slow "wriggling" we observe of the saturated aggregates (see Supplementary Material [16]). The experiments of Saragosti *et al* [12], which are performed in confined micro-channels and capillaries, show instead the development of traveling concentration waves of chemotactic bacteria. These traveling waves were initiated in the experiments through an initial concentration by centrifugation of the swimmer population to one end of the channel. We do not observe the spontaneous formation of such traveling waves here though ours is an open system (though confined geometrically by the assumed periodicity length) and the initial swimmer state is un-oriented and nearly homogeneous. The combined effects of a confining geometry and the initial concentration of swimmers has yet to be examined in our theoretical system.

We have shown that the intrinsically generated fluid flows arising from collective swimming of microorganisms can modify patterns of chemotactic aggregation and, most importantly, can limit aggregate concentration. This is unlike chemotactic models that predict concentration blow-up or include artificial terms to cap growth. While we have emphasized hydrodynamic effects in attractive chemotactic dynamics, it is important to remember that ours is a dilute to semi-dilute theory that does not capture near-interactions between swimmers, hydrodynamic or otherwise. In denser suspensions swimmer size limits local swimmer density through steric interactions though as yet well-founded models that combine these with hydrodynamic interactions do not exist.

Nonetheless, we expect similar results when large-scale coherence is driven by steric effects [10, 19]. On that note, steric effects with no hydrodynamics may also limit aggregation of chemotactic random walkers [20].

Finally, these auto-chemotactic effects can be seen as complementary to the enhanced mixing by swimmers [11] that has also been explored for microfluidic applications [21]. Systematic studies of the interplay between chemotaxis and locomotion-generated fluid flow should be possible through controlled introduction of exogeneous chemoattractants to trigger aggregation, through the interplay of quorum sensing and chemotaxis [22], and perhaps by specific genetic engineering of the dynamics of locomotion and chemosensing [23].

[1] C. Dombrowski, *et al.*, Phys. Rev. Lett. **93**, 098103 (2004); L.H. Cisneros, *et al.*, Exp. Fluids **43**, 737 (2007).
[2] S. Ramaswamy, Ann. Rev. Condens. Matter Phys. **1**, 323 (2010).
[3] E.O. Budrene and H.C. Berg, Nature **349**, 630 (1991).
[4] B.L. Bassler, Cell **109**, 421 (2002).
[5] E.F. Keller, L.A. Segel, J. Theor. Biol. **30**, 225 (1971).
[6] H.C. Berg, *Random Walks in Biology* Princeton University Press, 1993
[7] R.N. Bearon, T.J. Pedley, Bull. Math. Bio. **62**, 775 (2000).
[8] K.C. Chen, *et al.*, J. Math. Bio. **47**, 518 (2003).
[9] D. Saintillan and M.J. Shelley, Phys. Rev. Lett. **100**, 178103 (2008); also Phys. Fluids **20**, 123304 (2008).
[10] L.H. Cisneros, *et al.*, Phys. Rev. E **83**, 061907 (2011).
[11] E. Lushi and M.J. Shelley, preprint (2012).
[12] J. Saragosti, *et al.*, Proc. Natl. Acad. Sci. USA **108**, 16235 (2011).
[13] R. Stocker, *et al.*, Proc. Natl. Acad. Sci. USA **105**, 4209 (2008).
[14] R.M. Macnab and D.E. Koshland, Proc. Natl. Acad. Sci. USA **69**, 2509 (1972); N. Mittal, *et al.*, Proc. Natl. Acad. Sci. USA **100**, 13259 (2003).
[15] G.B. Jeffery, Proc. R. Soc. London, Ser. A **102**, 161 (1922).
[16] See Supplementary Material at [URL to be inserted by publisher] for movies of the swimmer concentration.
[17] S. Childress and J.K. Percus, Math. BioSci. **56**, 217 (1981).
[18] M.J. Schnitzer, *et al.*, Symp. Soc. Gen. Microbiol **46**, 15 (1990).
[19] K. Drescher, *et al.*, Proc. Natl. Acad. Sci. USA **108**, 10940 (2011).
[20] J. Taktikos, *et al.*, Phys. Rev. E **85**, 051901 (2012).
[21] M.J. Kim and K.S. Breuer, Anal. Chem. **79**, 955 (2007).
[22] S. Park, *et al.*. Science **301**, 188 (2003).
[23] C. Liu, *et al.*. Science **334**, 238 (2011).